Electrochemical Doping of Chirality-Resolved Carbon Nanotubes

Ladislav Kavan,*,† Martin Kalbáč,‡ Markéta Zukalová,† and Lothar Dunsch‡

J. Heyrovský Institute of Physical Chemistry, Academy of Sciences of the Czech Republic, Dolejškova 3, CZ-182 23 Prague 8, Czech Republic, and Leibniz Institute of Solid State and Materials Research, Helmholtzstr. 20, D-01069 Dresden, Germany

Received: June 1, 2005; In Final Form: August 6, 2005

Raman spectra of electrochemically charged single-wall carbon nanotubes (HiPco) were studied by five different laser photon energies between 1.56 and 1.92 eV. The bands of radial breathing modes (RBM) were assigned to defined chiralities by using the experimental Kataura plot. The particular (*n*,*m*) tubes exhibit different sensitivity to electrochemical doping, monitored as the attenuation of the RBM intensities. Tubes which are in good resonance with the exciting laser exhibit strong doping-induced drop of the RBM intensity. On the other hand, tubes whose optical transition energy is larger than the energy of an exciting photon show only small changes of their RBM intensities upon doping. This rule presents a tool for analysis of mixtures of single-walled carbon tubes of unknown chiralities. It also asks for a re-interpretation of some earlier results which were reported on the diameter-selectivity of doping. The radial breathing mode in strongly n- or p-doped nanotubes exhibited a blue-shift. A suggested interpretation follows from the charging-induced structural changes of SWCNTs bundles, which also includes a partial de-bundling of tube ropes.

1. Introduction

Raman spectra of single-wall carbon nanotubes (SWCNTs) are strongly resonant-enhanced via the optical transition between van Hove singularities (vHs).[1] This also provides a method for mapping of electronic structure and optical properties of SWCNTs. Electrochemical charging of SWCNTs allows further upgrade of this methodology by defined tuning of the electronic structure of SWCNTs, thus addressing the doping-induced changes of the Raman spectra in-situ.[2−8] The most obvious effect upon electrochemical doping is the attenuation of Raman intensities when the optical transitions between vHs are bleached, either by inserting extra electrons into the conduction band singularities (n-doping) or holes into the valence band singularities (p-doping).[2−8]

Samples of SWCNTs, produced in a variety of preparative methods, contain both metallic and semiconducting tubes of variable chiral indices (*n*,*m*), and these tubes are usually assembled in bundles. Except for a few studies on one isolated SWCNT,[2,3] all spectroelectrochemical works carried out to date had supplied convoluted information about a mixture of tubes.[4−8] However, recent advances in Raman, optical, and photoluminescence spectroscopy of surfactant-wrapped SWCNTs revealed accurate relations between the optical transition energies and the Raman radial breathing mode (RBM).[9−12] The correlation of RBM frequencies with the empirical values of optical transition energies (the so-called "experimental Kataura plot")[9−11] allows a unique (*n*,*m*) assignment, particularly for narrow semiconducting tubes of diameters between about 0.7 and 1.2 nm. The latter occur, for example, in the tubes made by a high-pressure catalytic decomposition of carbon monoxide (HiPco).

Charge-transfer processes, employing inorganic[13] or organic[14] acceptor molecules as well as O_2-mediated acid-basic reactions,[15] have been studied in detail with aqueous solutions of surfactant-wrapped HiPco tubes. Optical absorbance, Raman, and fluorescence spectra of (*n*,*m*)-resolved semiconducting tubes provided consistent evidence that the charge-transfer is chirality-selective. In particular, semiconducting tubes show an increase of the redox potential with increasing band gap.[13−15] Within the simplest tight-binding approximation, the energy separation of *i*th singularities, ΔE_{ii}, is inversely proportional to the tube diameter, *d*:

$$\Delta E_{ii} = \frac{2i\gamma_0 a_{CC}}{d} \quad (1)$$

where γ_0 is the nearest-neighbor overlap integral ($\approx$2.5 eV) and a_{CC} is the CC bond length ($\approx$142 pm). Due to curvature and many-body effects, the tight-binding model is perturbed, especially for narrow tubes ($d \approx <1.2$ nm).[12] Nevertheless, for the discussion presented below, we can neglect the deviations of ΔE_{ii} from the predicted $1/d$ behavior (eq 1) for smaller *d*. Spectroelectrochemistry on one isolated surfactant-wrapped tube[2,3] and chemical oxidation of tubes in solution[13,14] indicate that the position of the Fermi level (and band edges) scale linearly with ΔE_{ii}.[2,3,14] In other words, narrow tubes should be stronger reductants (easily oxidizable), whereas wide tubes should be stronger oxidants (easily reducible) (eq 1).

There are less detailed data on redox reactions of surfactant-free tubes in the solid phase, as these samples can hardly be investigated by fluorescence spectroscopy. Hence, the method of first choice is Raman spectroscopy, which, however, provides information on the band energetics only indirectly, via the resonance enhancement. Doping is carried out by the reaction of solid HiPco tubes with gaseous[16−18] or liquid[19] redox-active molecules, as well as electrochemically.[7,8] After charge-transfer, the compensating counterion is assumed to be located at the outer surface of the tube, but small gaseous molecules can also penetrate into the interior of a tube.[20] Recently, Iijima et al.[21]

* Corresponding author. E-mail: Kavan@jh-inst.cas.cz.
† J. Heyrovský Institute of Physical Chemistry, Academy of Sciences of the Czech Republic.
‡ Leibniz Institute of Solid State and Materials Research.

10.1021/jp052910e CCC: $30.25
Published on Web 10/05/2005

reported even on entrapping of aqueous electrolyte solutions in the interior of oxidatively decapped HiPco tubes. The intratubular electrolyte caused reversible and diameter-selective vanishing of RBM intensity, but details on charge-transfer from intratubular species are still unknown.[21]

First reports[16−18] on diameter-selective doping dealt with the reaction of gaseous $FeCl_3$ or K with bundled HiPco tubes. The sensitivity to doping was monitored by the relative attenuation of the RBM intensity in spectra excited at 2.41 and 1.83 eV.[16−18] At these conditions, the doping-sensitivity was minimal for tubes of diameters from 0.9 to 1.2 nm, but increased both for narrower and thicker tubes outside this region. We have reproduced this trend by in-situ Raman spectroelectrochemistry at 2.41-eV excitation, and have, moreover, found that the relative RBM attenuation also depends on the electrolyte counterion, which compensates the electronic charge at SWCNTs.[8] While the counterion-sensitivity of n-doping expectedly correlated with the size of the charge-compensating ion,[8] the nonmonotonic diameter-selectivity in doping was interpreted by more complex and somewhat inconsistent arguments.[8,16−18] Apparently, the nonmonotonic doping/diameter correlation[8,16−18] would contradict the conclusion that the redox potential of nanotubes is a linear function of the band gap (or inverse diameter).[14] Recent study of chemical p-doping with liquid HNO_3 and H_2SO_4 did not confirm the nonmonotonic diameter-selectivity of doping, either.[19] Raman spectra were interpreted in terms of variations in the resonance condition caused by Fermi level shift into the valence band.[19]

For further addressing these contradictions, the previous Raman studies[8,16−19] should be upgraded by employing (*n*,*m*) assignment from the experimental Kataura plot. Here we will show that the doping-induced attenuation of the RBM intensity is controlled primarily by the actual deviation of the optical transition energy of the particular (*n*,*m*) tube from the energy of the exciting photon, that is, by the accuracy of fulfilling of resonance conditions. This approach smoothly explains salient effects associated with the intensity modulations of RBMs in redox-doped nanotubes.

2. Experimental Section

The sample of HiPco nanotubes was available from our previous works.[7,8] Spectroelectrochemical experiments employed a Pt-supported thin film of nanotubes, which was fabricated by evaporation of a sonicated ethanolic slurry of nanotubes. The working electrode was outgassed overnight at 70 °C in a vacuum (10^{-1} Pa) and then mounted in a spectroelectrochemical cell in a glovebox under nitrogen. The cell was equipped with Pt-counter and Ag-wire pseudoreference electrodes; 0.2 M $LiClO_4$ in dry acetonitrile (Aldrich) was the electrolyte solution. The pseudoreference potential was calibrated after adding a small amount of ferrocene to the electrolyte solution at the end of each series of spectroelectrochemical tests. Hence, all potentials were referred to the ferrocene reference electrode, Fc/Fc^+. Electrochemical doping was carried out potentiostatically (PG 300-HEKA potentiostat). Bold lines in the Raman spectra (Figures 1−5) denote measurements at the applied potential of 0 V vs Ag-pseudoreference (−0.35 to −0.37 V vs Fc/Fc^+), which roughly corresponds to the undoped state of nanotubes. (Open-circuit potentials of the SWCNT-covered Pt electrode in a freshly assembled cell were between −0.2 and −0.4 V vs Fc/Fc^+). Spectra were excited by a Kr^+ laser (Innova 300 series, Coherent) or by a Ti−sapphire laser (899LC, Coherent) and recorded by a T-64000 spectrometer (Instruments, SA) interfaced to an Olympus BH2 microscope. The laser power impinging on the cell window was between 1 and 5 mW. The Raman spectrometer was calibrated before each set of measurements by using for reference the F_{1g} line of Si at 520.2 cm^{-1}. All frequencies and intensities at the given excitation were normalized against the Si line. A second convenient reference, both for intensities and frequencies, are the bands of acetonitrile at 378.5 and 1375.5 cm^{-1}, which serve as an internal standard in the spectroelectrochemistry of nanotubes.[7,8]

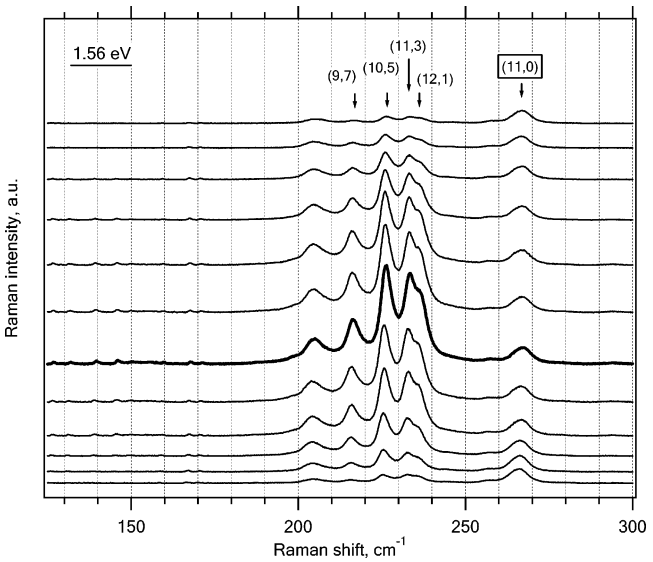

Figure 1. Raman spectra of HiPco nanotubes (excited by a Ti−sapphire laser at 1.56 eV) in 0.2 M $LiClO_4$ + acetonitrile. The electrode potential (in V vs Fc/Fc^+) was for curves from top to bottom: −1.55, −1.35, −1.15, −0.95, −0.75, −0.55, −0.35 (bold line), −0.15, 0.05, 0.25, 0.45, 0.65. Spectra are offset for clarity, but the intensity scale is identical. The tubes with large positive deviation from resonance condition (ΔE_R) are highlighted by a box-framed annotation. Bold line denotes a spectrum of nearly undoped sample, see Experimental Section for details.

3. Results and Discussion

In general, the intensity of Stokes resonant Raman scattering (I) scales with the laser photon energy, E_L, and the optical transition energy, E_{ii}:

$$I = \frac{c}{|(E_L - E_{ii} - i\gamma)(E_L + E_{ph} - E_{ii} - i\gamma)|^2} \qquad (2)$$

where E_{ph} is the phonon energy, and γ is the damping constant; typical values for RBM are $E_{ph} \approx 0.02$ eV and $\gamma \approx 0.05$ eV. Hence, the intensity of RBM is maximal if E_L approaches E_{ii}. At the used E_L from 1.56 to 1.92 eV (see Experimental Section), the semiconducting tubes with diameters of about 0.7−1.2 nm are in resonance via the optical transition between second vHs, E_{22}^S. Consequently, the energy difference:

$$\Delta E_R = E_{22}^S - E_L \qquad (2a)$$

is a parameter characterizing the deviation of a particular tube from the ideal resonance (eq 2).

Figures 1−5 show the spectroelectrochemical plots for HiPco tubes at five different values of E_L. Also shown is the (*n*,*m*) assignment for selected tubes, for which the experimental Kataura plot provides defined resolution of the given chirality at the selected E_L.[9−11] The spectral assignment is sometimes complicated by overlaps, such as (11,0) & (10,2) and (13,0) &

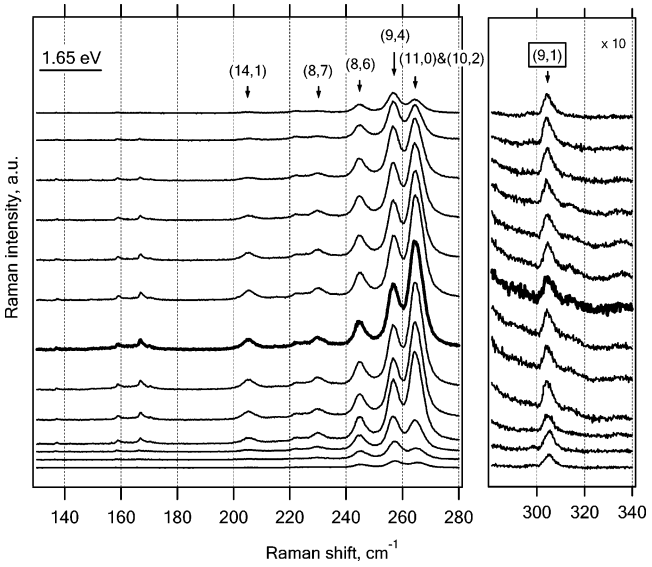

Figure 2. Raman spectra of HiPco nanotubes (excited by a Ti−sapphire laser at 1.65 eV) in 0.2 M $LiClO_4$ + acetonitrile. The electrode potential (in V vs Fc/Fc^+) was for curves from top to bottom: −1.57, −1.37, −1.17, −0.97, −0.77, −0.57, −0.37 (bold line), −0.17, 0.03, 0.23, 0.43, 0.63, 0.83. Spectra are offset for clarity, but the intensity scale is identical in the respective windows. Left chart shows the same spectra with intensity scale zoomed by a factor of 10. The tubes with large positive deviation from resonance condition (ΔE_R) are highlighted by a box-framed annotation. Bold line denotes a spectrum of nearly undoped sample, see Experimental Section for details.

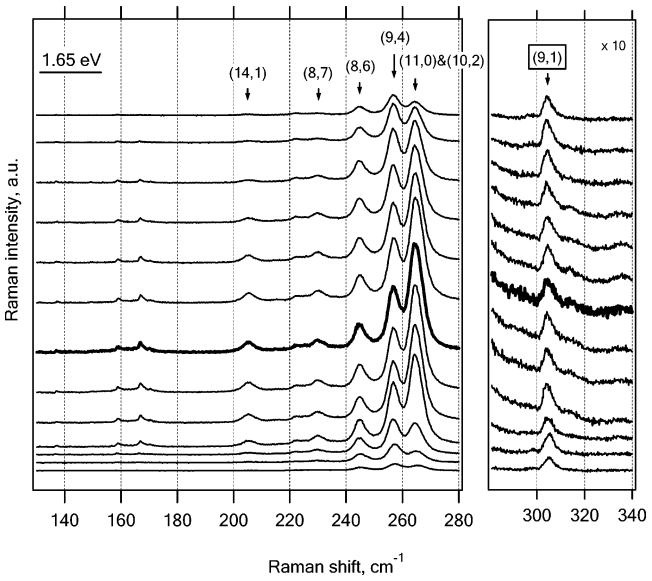

Figure 3. Raman spectra of HiPco nanotubes (excited by a Ti−sapphire laser at 1.75 eV) in 0.2 M $LiClO_4$ + acetonitrile. The electrode potential (in V vs Fc/Fc^+) was for curves from top to bottom: −1.56, −1.36, −1.16, −0.96, −0.76, −0.56, −0.36 (bold line), −0.16, 0.04, 0.24, 0.44, 0.64. Spectra are offset for clarity, but the intensity scale is identical in the respective window. The tubes with large positive deviation from resonance condition (ΔE_R) are highlighted by a box-framed annotation. Bold line denotes a spectrum of nearly undoped sample, see Experimental Section for details.

(12,2) & (8,7). Also, the (14,1) tube is poorly detectable at 1.56-eV excitation due to the overlap with (13,3) and (9,8). In general, the accuracy of the (*n*,*m*) assignment depends on how the RBM and ΔE_R for a given (*n*,*m*) tube diverge from the corresponding values for some other tube(s). The reported precision of RBM is now better than ± 1 cm^{-1} and for E_{22}^S (or ΔE_R) ± 10 meV (refs 9−11). Obviously, the (*n*,*m*) assignment is unique for tubes

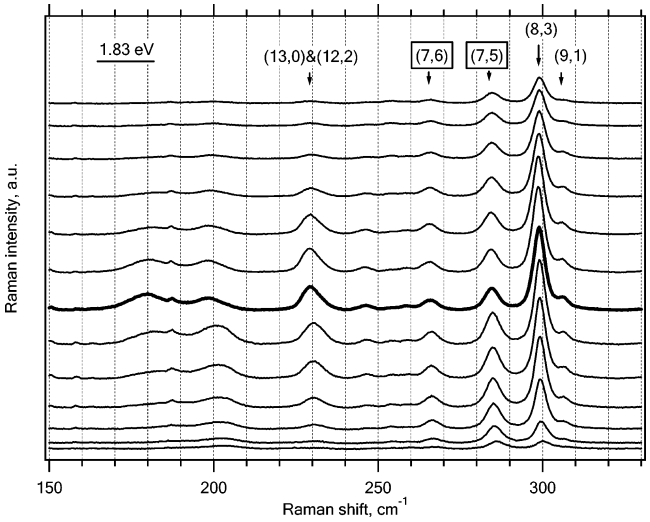

Figure 4. Raman spectra of HiPco nanotubes (excited by Kr^+ laser at 1.83 eV) in 0.2 M $LiClO_4$ + acetonitrile. The electrode potential (in V vs Fc/Fc^+) was for curves from top to bottom: −1.55, −1.35, −1.15, −0.95, −0.75, −0.55, −0.35 (bold line), −0.15, 0.05, 0.25, 0.45, 0.65, 0.85. Spectra are offset for clarity, but the intensity scale is identical. The tubes with large positive deviation from resonance condition (ΔE_R) are highlighted by a box-framed annotation. Bold line denotes a spectrum of nearly undoped sample, see Experimental Section for details.

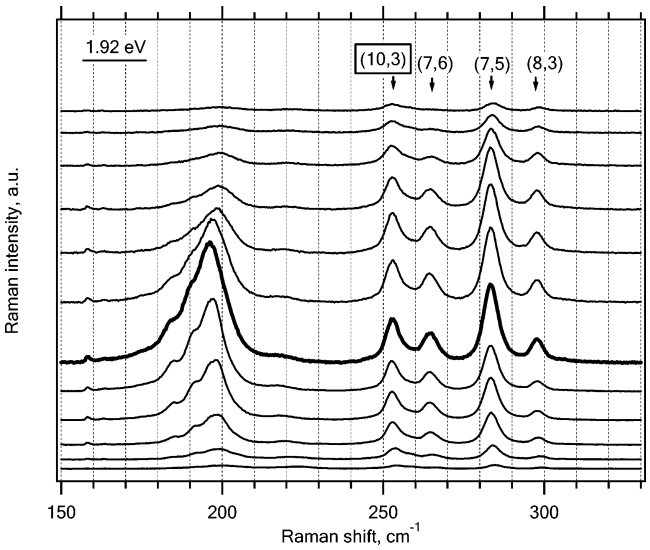

Figure 5. Raman spectra of HiPco nanotubes (excited by Kr^+ laser at 1.92 eV) in 0.2 M $LiClO_4$ + acetonitrile. The electrode potential (in V vs Fc/Fc^+) was for curves from top to bottom: −1.57, −1.37, −1.17, −0.97, −0.77, −0.57, −0.37 (bold line), −0.17, 0.03, 0.23, 0.43, 0.63. Spectra are offset for clarity, but the intensity scale is identical. The tubes with large positive deviation from resonance condition (ΔE_R) are highlighted by a box-framed annotation. Bold line denotes a spectrum of nearly undoped sample, see Experimental Section for details.

of small diameters and red or NIR lasers, because there are no other tubes, which would conflict in the nearby RBM−E_{22}^S region.

By employing this unique assignment (Figures 1−5), it turns out that the doping-induced attenuation of RBM is dependent on the quality of fulfillment of the resonance condition (ΔE_R; cf. eqs 2, 2a). To make a quantitative assessment, we shall neglect the small difference (ca. 70 meV) in E_{ii} for bundled and surfactant-wrapped nanotubes[11] and evaluate ΔE_R throughout from the literature data on wrapped SWCNTs.[9−11] Table 1 compiles the relevant values.

TABLE 1: Frequencies of the Radial Breathing Mode (ω_{RBM}) and Energies of the E_{22}^S Transitions of Selected Nanotubes, Which Were Identified in the Studied Raman Spectra (Figures 1−5)[a]

tube	ω_{RBM} (cm^{-1})	E_{22}^S (eV)[b]	E_{22}^S (eV)[c]	E_{22}^S (eV)[d]	$\varnothing E_{22}^S$ (eV)	ΔE_R(1.56) (eV)	ΔE_R(1.65) (eV)	ΔE_R(1.75) (eV)	ΔE_R(1.83) (eV)	ΔE_R(1.92) (eV)
(12,1)	237	1.552	1.55	1.551	1.55	−0.01				
(11,3)	232	1.564	1.57	1.570	1.57	0.01				
(9,7)	216	1.563	1.58	1.564	1.57	0.01				
(10,5)	225	1.574	1.58	1.578	1.58	0.02				
(14,1)	206	1.657	1.64		1.65	0.09[f]	0			
(11,0)	267	1.665		1.657	1.66	0.1	0.01			
(10,2)	265	1.683	1.68	1.690	1.68		0.03			
(8,7)	230	1.702	1.70		1.70		0.05	−0.05		
(9,4)	257	1.716	2.03[e]	1.72	1.72		0.07	−0.03		
(8,6)	245	1.727	1.72	1.73	1.73		0.08	0.02		
(9,1)	307	1.794	1.8	1.78	1.79		0.14	0.04	−0.04	
(12,2)	226	1.807			1.81			0.06	−0.02	
(13,0)	228	1.831			1.83			0.08	0	
(8,3)	298	1.863	1.86	1.857	1.86			0.11	0.03	−0.06
(7,5)	283	1.921	1.92	1.915	1.92			0.17	0.09	0
(7,6)	263	1.914	1.92		1.92				0.09	0
(10,3)	253	1.963	1.95		1.96					0.04

[a] The values were compiled from refs 9−11, and averaged energies, $\varnothing E_{22}^S$, are also shown; tubes are ordered according to the increasing $\varnothing E_{22}^S$; the deviation from the laser photon energy ($\Delta E_R = \varnothing E_{22}^S - E_L$) is shown for the five different laser photon energies used (photon energies, E_L, are in parentheses.) [b] Ref 10. [c] Ref 11. [d] Ref 9. [e] This value was not considered in evaluation. [f] The (14,1) tube is poorly detectable at 1.56 eV due to overlap with (13,3) and (9,8).

Our analysis provides consistent evidence that the tubes having large ΔE_R are sluggish in the doping-induced RBM attenuation. These tubes are highlighted in Figures 1−5 by a box-framed annotation. For instance, the tube (11,0) is almost doping-silent in Figure 1 ($\Delta E_R = 0.1$ eV), but doping-sensitive in Figure 2 ($\Delta E_R = 0.01$ eV). In the first case, the tube (11,0) is in poor resonance, exhibiting a weak and broad RBM band, which almost does not change upon doping (Figure 1). Analogously, the poorly resonating tubes (9,1), (8,6), and (9,4) in Figure 2 respond weakly to doping, compared to tubes (14,1), (11,0), and (10,2), which are in good resonance. Tube (9,1) is nearly doping-silent in Figure 2 ($\Delta E_R = 0.14$ eV), but strongly doping-sensitive in Figure 3 ($\Delta E_R = 0.03$ eV). Another explicit example is tube (7,5), which is doping-silent in Figure 3 ($\Delta E_R = 0.17$ eV), medium-sensitive in Figure 4 ($\Delta E_R = 0.09$ eV), and highly sensitive in Figure 5 ($\Delta E_R = 0$).

A more detailed evaluation of doping-sensitivity of the particular (*n*,*m*) tubes follows from the analysis of normalized RBM intensity on the applied electrochemical potential. Figure 6 displays the intensity/potential profiles for the four used E_L values from 1.56 to 1.83 eV. The data for the 1.92-eV laser are not shown, as there is no unique assignment for a tube having a large ΔE_R (a possible candidate would be (11,1), but this tube is not clearly traceable in Figure 5). All charts in Figure 6 are organized in the same way, that is, the increasing ΔE_R is coded by the particular color in the series: magenta (lowest ΔE_R) < green < blue < red < black (highest ΔE_R). As expected, the black and red curves represent the broadest doping profiles, albeit these curves are also somewhat more noisy due to zooming of experimental errors by normalization of the relatively weak Raman intensities.

This resonance-selection rule is qualitatively understood. The tube, which is in perfect resonance ($\Delta E_R = 0$), is extremely sensitive to the changes in population of the vHs, between which the photoselective optical transition occurs. On the other hand, tubes with $\Delta E_R \rightarrow \infty$ are intact if the transitions change, because the resonance enhancement is not operating any more. (The latter situation is reminiscent of the behavior of a heavily n-doped nanotube. In this case, the optical transitions are fully quenched due to the complete filling of the relevant vHs, causing the Raman scattering to be nonresonant, either. The RBM intensities are thus attenuated by orders of magnitude, but the RBM profile then directly reflects the distribution of tube diameters.[22]) The nonresonant Raman scattering is hardly traceable by the Raman spectroelectrochemistry, but tubes which are in weak resonance ($\Delta E_R \approx 0.1$ eV) are convenient for monitoring of intermediate feedback between these two extremes.

There are two other subtle effects which contribute to the observed dependence of doping-sensitivity on ΔE_R. Tubes which are out of resonance toward positive ΔE_R have larger E_{22}^S (cf. Table 1) and therefore require larger electrochemical potentials (driving force) for bleaching of the corresponding optical transitions. If we assume for simplicity that the Fermi energy is in the middle of the band gap,[14] then the additional energy required for filling/depleting of the vHs states by cathodic/anodic charging is $\Delta E_R/2$, referred to the energy for the vHs filling/depleting in a perfectly resonating tube. Therefore, the applied cathodic or anodic potential for a tube with $\Delta E_R > 0$ must be larger to achieve the same electron or hole transfer as for the perfectly resonating tube ($\Delta E_R = 0$).

A second effect, which contributes to the weaker doping-feedback of tubes with larger ΔE_R, is the red-shift of E_{22}^S upon doping.[14] Although this red-shift is significantly dependent on the tube environment[14] and there is a lack of relevant data for electrochemical doping, we can consider it as a synergic mechanism explaining our resonance rule. The red-shift would cause the tubes having large ΔE_R to become more resonant because ΔE_R is decreased, but tubes with $\Delta E_R \rightarrow 0$ are brought out of resonance.[14] Nevertheless, the redox chemistry of nanotubes in solution[13−15] should be transferred with care to the electrochemistry of nanotube films on metallic supports. The most obvious problem is the tube−tube interaction in a bundle and the tube−substrate interaction, which equilibrate the Fermi level positions of all the contacting solids.

Our "resonance rule" asks for a re-interpretation of the previously published data on chemical doping.[16−18] At the 1.83-eV excitation, the lowest doping-sensitivity was observed for a tube with RBM = 265 cm^{-1} (refs 17,18). If we assign this tube to (7,6), the cited results[16−18] can be smoothly rationalized by our resonance rule (cf. Figure 4) rather than by the formerly suggested "diameter-selectivity" of doping.[16−18] Obviously, the

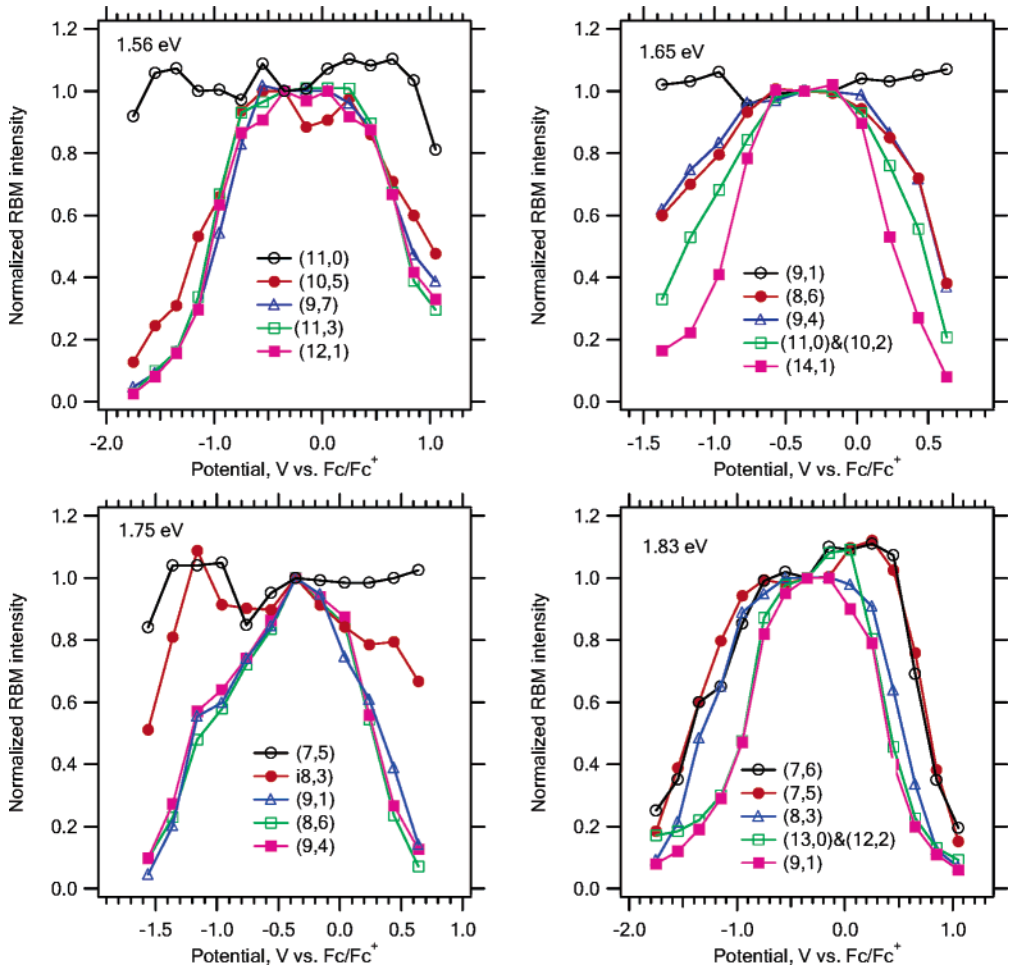

Figure 6. Intensity of the RBM line as a function of the applied electrochemical potential in 0.2 M $LiClO_4$ + acetonitrile at four different excitation laser energies (1.56 to 1.83 eV). The intensities were normalized by assigning 1 to the RBM intensity at 0 V vs Ag-wire (−0.35 to −0.37 V vs Fc/Fc^+; bold curves in Figures 1−5). The increasing ΔE_R is coded as follows: magenta—full squares (lowest ΔE_R) < green—open squares < blue—triangles < red—full circles < black—open circles (highest ΔE_R). Assignment of the curves to the particular (*n*,*m*) tubes is also labeled.

diameter-selectivity rule is accidentally valid at 1.83-eV excitation, but not at other excitation energies, for example, at 1.56 eV (cf. Figures 1 and 4). Our treatment also suggests a tool for the estimation of transition energies. For instance, the (8,3) tube is highly doping-sensitive at 1.83 eV, and the (9,1) tube is highly doping-sensitive at 1.75 eV (Figures 3, 4, 6). This would predict that the $E_{22}^S(8,3)$ is larger than $E_{22}^S(9,1)$, which is in full agreement with recent calculations and independent experiments (Table 1).

Doorn et al.[14] reported on chiral-selective bleaching of optical transitions upon reaction of HiPco tubes with organic acceptor molecules, such as 4-amino-1,1′-azobenzene-3,4′-disulfonic acid. The Raman spectra of azobenzene-oxidized tubes (excited at 1.58 eV; cf. Figure 5 in ref 14) are comparable to our spectra of anodically oxidized tubes excited at 1.56 eV (Figure 1). In both cases, the band at 265 cm^{-1} is the least-affected one by p-doping. It is interesting to note that a qualitatively identical effect can be traced also in the Raman spectra of tubes that had been covalently derivatized by the 4-*tert*-butylphenyl group.[23] Figure 6 in ref 23 gives evidence that the RBM intensity at about 265 cm^{-1} (1.59-eV excitation) is less attenuated in comparison with the RBM intensities of the remaining (wider) tubes in this resonance window. Covalent functionalization removes π-electrons from graphene, because the bonding site transforms from sp^2 to sp^3 hybridization.[23] Hence, this process is reminiscent of p-doping, and we can suggest that it is also chiral-selective.

In this context, we should note that the doping-induced RBM attenuation is of electronic origin and has no implication for the concentration or structural perfectness of (*n*,*m*) tubes. The electrochemical charging causes only reversible changes of the electronic state (unless we apply extreme potentials, when the tubes may decompose chemically[7]). The purely electronic nature of the RBM attenuation is explicitly illustrated by the insensitivity of the 265-cm^{-1} band at 1.56−1.59 eV-excitation (see previous paragraph). Note that if we think of chemical breakdown reactions, the narrowest tubes (265-cm^{-1} band) should be just the most reactive ones, which is virtually opposite to our resonance rule. For instance, upon ozonolysis, the narrow tubes show greater loss of resonance enhancement of RBM than wider tubes at 1.59-eV excitation.[24] Analogously, high doping with concentrated H_2SO_4 caused marked attenuation of all RBM bands (at 1.59-eV excitation) including the 265-cm^{-1} band, but low doping with H_2SO_4 did not affect the 265-cm^{-1} band that dramatically (cf. Figure 6c in ref 19). We can suggest that the low H_2SO_4 doping reflects mostly electronic changes, whereas high H_2SO_4 doping causes also chemical changes of the tube. In other words, the mild H_2SO_4-doping is diameter-selective only indirectly (via the resonance-selection rule), but the heavy H_2SO_4-doping reflects the diameter-selectivity directly (via the differential reactivity of narrow/wide nanotubes).

At the 2.41-eV excitation, the lowest doping-sensitivity was traced for tubes near RBM ≈ 245 cm^{-1}, both for chemical doping[16−18] and for electrochemical doping.[8] We attribute this

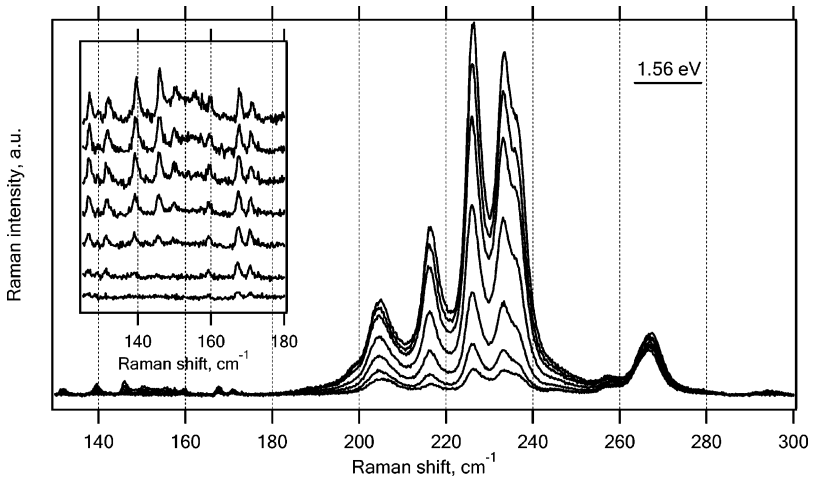

Figure 7. Raman spectra of HiPco nanotubes (excited by a Ti−sapphire laser at 1.56 eV) in 0.2 M $LiClO_4$ + acetonitrile. The electrode potential (in V vs Fc/Fc^+) was for curves from bottom to top: −1.55, −1.35, −1.15, −0.95, −0.75, −0.55, −0.35. Inset shows selected region of spectra with zoomed intensity scale and offset for clarity.

to another accidental matching of resonance-selectivity with the previously reported[8,16−18] diameter-selectivity. Since, however, the 2.41-eV photons resonate with too many tubes via the transitions E_{22}^S, E_{33}^S, and E_{11}^M, the spectra are not that easily assignable to unique chiral indices as are those for the red lasers. We can only speculate that the largest observable RBM ≈ 312 cm^{-1} in the previously published spectra[8,16,17] seems to be assignable to the (7,3) tube, which is in good resonance with the green laser ($\Delta E_R = 0.05$ eV).[10]

Our resonance rule can be used as a diagnostic tool for analysis of a mixture of tubes of unknown chiralities. This is demonstrated in Figure 7, which shows an example of a spectroelectrochemical plot zoomed in the area of metallic tubes, E_{11}^M, and also wide semiconducting tubes, E_{33}^S. Even though the exact spectral assignment is not yet proved, we can classify tubes according to their sensitivity to the charging-induced drop of the RBM intensity. From there, we can predict that the tubes with RBM = 167 and 171 cm^{-1} are in poorer resonance, having $E_{11}^M > E_L = 1.56$ eV, whereas the tubes with RBM = 140, 150, and 156 cm^{-1} are in good resonance with $E_L = 1.56$ eV (Figure 7, inset).

It is challenging to explore whether our resonance rule is applicable for analysis of inner tubes in the double-wall carbon nanotubes. For instance, the RBM spectra excited at 1.83 eV were previously assigned to the following inner tubes: (11,0), (8,4), (7,5), (9,2), and (10,0), as well as to metallic tubes, exhibiting, according to the ab-initio calculations, optical transitions for energies lower than E_{11}^M (ref 25). We have tested their doping-sensitivity; we found that the tubes assigned as (8,4) and as metallic ones are almost doping-silent compared to the remaining tubes.[26] Unfortunately, the tube assigned as (8,4) would be too far from resonance ($\Delta E_R = 0.27$ eV);[10] the same is true for the remaining tubes listed above, except for the (7,5) tube ($\Delta E_R = 0.09$ eV). Obviously, there seems to be some problem with the published[25] (*n*,*m*) assignment of inner tubes, but addressing these questions is beyond the scope of this paper. We can only mention a recent study by Pfeiffer et al.[27] showing that the found number of RBM bands of inner tubes is larger than expected from the experimental Kataura plot.

Besides the intensity of RBM, the peak position also provides interesting information. Figures 1−5 evidence that the peaks, assignable to defined (*n*,*m*) tubes, do not show any marked frequency shifts at "reasonable" charging, that is, at potentials between about −1.2 and 0.4 V vs Fc/Fc^+. However, there is a pronounced tendency of certain RBM peaks to blue-shift at larger cathodic or anodic potentials: see, for instance, tube (9,1) in Figure 3 and tube (7,5) in Figure 5. This shift is partly reversible at the back-scan to smaller potentials. The blue-shift is about 1−2 cm^{-1} at the conditions used, but is not identical for all tubes. The origin of this blue-shift is not clear yet. Phenomenologically, it may simply follow from the CC bond-length contraction, which is also mirrored by blue-shifts of the tangential displacement mode (G-band).[28] Unfortunately, the relations between CC bond-length and doping are poorly understood, especially for n-doping.[28]

We may also consider the influence of tube environment, which is involved in the well-known dependence of RBM frequency (ω_{RBM}) on the tube diameter (d):

$$\varpi_{RBM} = \frac{c_1}{d} + c_2 \tag{3}$$

where c_1 and c_2 are constants. Equation 3 should be more rigorously formulated by considering the curvature effect:[12]

$$\varpi_{RBM} = \frac{A}{d} + B + \frac{C + D\cos^2 3\Theta}{d^2} \tag{4}$$

where θ is the chiral angle, and A, B, C, and D are constants. The effect of tube environment is quantified by the value of B (or by the values of c_2 in eq 3). It is considered to be zero for an isolated tube, but ≈10 cm^{-1} for bundled tubes and ≈8−19 cm^{-1} for surfactant-wrapped tubes.[1,9,12] If we assume A, C, and D to be invariant of environment, the surfactant wrapping may cause a small blue-shift compared to bundled SWCNTs. (However, some authors have reported that these ω_{RBM} shifts are negligible, too[11]). Our data would indicate that B further increases if the surfactant is replaced by a large number of ions compensating the electronic charge at SWCNTs. If the doping is strong enough, the ions are located not only at the outer surface of bundles but also in the voids between individual SWCNTs in a bundle. This matches the fact that the RBM upshifts abruptly at a certain threshold potential. At this stage, the tubes are debundled to some extent, and the tube−tube interaction ($B \approx 10$ cm^{-1}) is replaced by tube−ion interactions ($B > 10$ cm^{-1}). Eventually, strongly n-doped tubes dissolve in some organic solvents, and this can be interpreted as a result of debundling via tube−ion interactions, too.[29] Even stronger tube−ion interactions could be assumed if the nanotubes are

covalently derivatized by anchoring of surface ionic groups. Indeed, blue-shifts of RMB of about 8 cm^{-1} were traced for HiPco tubes, which had been functionalized by surface carboxyl groups.[18]

4. Conclusions

In-situ Raman spectroelectrochemistry of (*n*,*m*) resolved HiPco nanotubes indicates that the previously reported non-monotonic diameter-sensitivity of doping needs revision. In fact, the "diameter-selectivity rule" is valid accidentally at certain laser energies only. The actual mechanism, which controls the doping-sensitivity of SWCNTs, is the resonance condition. Tubes which are in good resonance are also doping-sensitive. On the other hand, tubes whose optical transition energy is larger than that needed for perfect fulfilling of the resonance condition, respond less strongly to doping.

This rule allows distinction of tubes which are in good resonance from tubes which are in weaker resonance with the exciting laser. As the transition energies are now known for many (*n*,*m*) resolved tubes with good precision, our new "resonance-selection rule" presents a tool for an analysis of mixtures of tubes of unknown chiralities. Whereas this procedure is well applicable to SWCNTs, the analysis of inner tubes in double-wall carbon nanotubes still requires further clarification. Obviously, chirality assignment of inner tubes in DWCNTs is a crucial problem to be addressed.

The RBM frequencies of strongly n- or p-doped SWCNTs tend to exhibit blue-shift. Suggested interpretation follows from the charging-induced CC-bond contraction and from breaking of van der Waals forces, which keep the SWCNTs cohering in bundles. The blue-shift is more pronounced for certain chiralities in a mixture of tubes.

Acknowledgment. This work was supported by IFW Dresden, Academy of Sciences of the Czech Republic (Contract No. A4040306) and by Czech Ministry of Education Youth and Sports (Contract No. LC-510).

References and Notes

(1) Dresselhaus, M. S.; Dresselhaus, G.; Saito, R.; Jorio, A. *Phys. Rep.* **2005**, *409*, 47.

(2) Okazaki, K.; Nakato, Y.; Murakoshi, K. *Phys. Rev. B* **2003**, *68*, 035434.

(3) Okazaki, K.; Nakato, Y.; Murakoshi, K. *Surf. Sci.* **2004**, *566*−*568*, 436.

(4) Corio, P.; Santos, P. S.; Brar, V. W.; Samsonidze, G. G.; Chou, S. G.; Dresselhaus, M. S. *Chem. Phys. Lett.* **2003**, *370*, 675.

(5) Stoll, M.; Rafailov, P. M.; Frenzel, W.; Thomsen, C. *Chem. Phys. Lett.* **2003**, *375*, 625.

(6) Kavan, L.; Dunsch, L.; Kataura, H. *Carbon* **2004**, *42*, 1011.

(7) Kavan, L.; Rapta, P.; Dunsch, L.; Bronikowski, M. J.; Willis, P.; Smalley, R. E. *J. Phys. Chem. B* **2001**, *105*, 10764.

(8) Kavan, L.; Dunsch, L. *Nano Lett.* **2003**, *3*, 969.

(9) Telg, H.; Maultzsch, J.; Reich, S.; Hennrich, F.; Thomsen, C. *Phys. Rev. Lett.* **2004**, *93*, 177401.

(10) Weisman, R. B.; Bachilo, S. M. *Nano Lett.* **2003**, *3*, 1235.

(11) Fantini, C.; Jorio, A.; Souza, M.; Strano, M. S.; Dresselhaus, M. S.; Pimenta, M. A. *Phys. Rev. Lett.* **2004**, *93*, 147406.

(12) Jorio, A.; Fantini, C.; Pimenta, M. A.; Capaz, R. B.; Samsonidze, G. G.; Dresselhaus, G.; Dresselhaus, M. S. *Phys. Rev. B* **2005**, *71*, 075401.

(13) Zheng, M.; Diner, B. A. *J. Am. Chem. Soc.* **2004**, *126*, 15490.

(14) O'Connell, M. J.; Eibergen, E. E.; Doorn, S. K. *Nat. Mater.* **2005**, *4*, 412.

(15) Strano, M. S.; Huffman, C. B.; Moore, V. C.; O'Connell, M. J.; Haroz, E. H.; Hubbard, J.; Miller, M.; Rialon, K.; Kittrell, C.; Ramesh, S.; Hauge, R. H.; Smalley, R. E. *J. Phys. Chem. B* **2003**, *107*, 6979.

(16) Kukovecz, A.; Pichler, T.; Pfeiffer, R.; Kuzmany, H. *Chem. Commun.* **2002**, 1730.

(17) Kukovecz, A.; Pichler, T.; Kramberger, C.; Kuzmany, H. *Phys. Chem. Chem. Phys.* **2003**, *5*, 582.

(18) Kuzmany, H.; Kukovecz, A.; Simon, F.; Holzweber, M.; Kramberger, C.; Pichler, T. *Synth. Met.* **2004**, *141*, 113.

(19) Zhou, W.; Vavro, J.; Nemes, N. M.; Fischer, J. E.; Borondics, F.; Kamaras, K.; Tanner, D. B. *Phys. Rev. B* **2005**, *71*, 205423.

(20) Kalbac, M.; Kavan, L.; Zukalova, M.; Dunsch, L. *J. Phys. Chem. B* **2004**, *108*, 6275.

(21) Zheng, M.; Yudasaka, M.; Iijima, S. *J. Phys. Chem. B* **2005**, *109*, 6037.

(22) Pichler, T.; Kuzmany, H.; Kataura, H.; Achiba, Y. *Phys. Rev. Lett.* **2001**, *87*, 267401.

(23) Bahr, J. L.; Yang, J.; Kosynkin, D. V.; Bronikowski, M. J.; Smalley, R. E.; Tour, J. M. *J. Am. Chem. Soc.* **2001**, *123*, 6536.

(24) Banerjee, S.; Wong, S. S. *Nano Lett.* **2004**, *4*, 1445.

(25) Pfeiffer, R.; Kuzmany, H.; Kramberger, C.; Schaman, C.; Pichler, T.; Kataura, H.; Achiba, Y.; Kürti, J.; Zolyomi, V. *Phys. Rev. Lett.* **2003**, *90*, 225501.

(26) Kavan, L.; Kalbac, M.; Zukalova, M.; Krause, M.; Dunsch, L.; Kataura, H. *Fuller. Nanotub. Carbohydr. Nanostruct.* **2005**, *13*, 115.

(27) Pfeiffer, R.; Simon, F.; Kuzmany, H.; Popov, V.N. In *Proceedings of the XIX International Winterschool on Electronic Properties of Novel Materials*; Kuzmany, H., Fink, J., Mehring, M., Roth, S., Eds.; Kirchberg/Tirol, Austria, 2005; pp 99.

(28) Chen, G.; Furtado, C. A.; Bandow, S.; Iijima, S.; Eklund, P. C. *Phys. Rev. B* **2005**, *71*, 045408.

(29) Penicaud, A.; Poulin, P.; Derre, A.; Anglaret, E.; Petit, P. *J. Am. Chem. Soc.* **2005**, *127*, 8.